Induced Tissue Cell Death by Magnetic Nanoparticle Hyperthermia for Cancer Treatment: An *in silico* Study

M. Saeedi, O. Vahidi *

School of Chemical Engineering, Iran University of Science and Technology, Narmak, P. O. Box: 16846, Tehran, Iran

ARTICLE INFO	ABSTRACT
	In this paper, we simulate magnetic hyperthermia process on a mathematical phantom model representing cancer tumor and its surrounding healthy tissues. The temperature distribution throughout the phantom model is obtained by solving the bio-heat equations, and the consequent cell death amount is calculated using the correlations between the tissue local temperature and the cell death rate. To obtain an estimate of the heat generated from typical magnetic nanoparticles, magnetite nanoparticles are synthesized, and the heat dissipation amount from the synthesized nanoparticles exposed to an alternating magnetic field is measured and used in the computer simulation. The impact of the amount of heat generated from the magnetic nanoparticles exposed to an alternating magnetic field and their distribution patterns in the tumor and hyperthermia process duration time on the cell death rate in both cancer and healthy tissues are investigated. It is indicated that while various factors contributing to the amount of the heat dissipation from the magnetic nanoparticles are important in the effectiveness of the magnetic hyperthermia process, the distribution pattern plays a major role in determining the efficiency of the process.

1. Introduction

Magnetic nanoparticles (MNPs) are progressively and extensively used in various medical applications including magnetic cell sorting, magnetic drug delivery, magnetic resonance imaging (MRI), and magnetic hyperthermia for cancer treatment [1-5]. Magnetic nanoparticle hyperthermia combined with the anti-cancer drug targeted delivery to the tumor tissue is becoming an emerging approach in cancer therapy due to its effectiveness and non-invasive nature with minor side effects [6-9]. In this approach, the MNPs dispersed in a fluid, called nanofluid, are used as the drug carriers and heat-generating elements into the target tissue. They are either directly injected or guided into the target tissue, and by implementing external alternative magnetic field, the tissue is locally heated up to 45 ^{o}C [10]. Since the cancer cells are more vulnerable to high temperature compared with the healthy cells [11, 12], the elevated temperature induces local cancer tissue cells death synergized by

*Corresponding author: ovahidi@iust.ac.ir

higher amount of anti-cancer drug release (at a high temperature) leading to the local destruction of the cancer tissue with a minimal damage to the surrounding healthy tissues. Hyperthermia in higher temperatures (above 50 ^{o}C), called thermo-ablation, is also investigated in few studies on laboratory animals with successful results [13].

Several factors contribute to the magnetic nanoparticle hyperthermia process including the MNPs chemical composition, concentration, mean diameter and shape, distribution pattern of MNPs within the tumor tissue, frequency and intensity of the magnetic field, duration of hyperthermia process, and physical properties of the target tissue [14]. To have an optimal thermotherapy with maximum damage to the cancer tissue cells and with minimal harm to the surrounding tissues, the optimum value for each mentioned factor has to be determined. Evaluating the effect of each factor on the hyperthermia process requires designing and performing several expensive experiments which is not cost effective. Computer simulation is an inexpensive alternative to the experimentation which provides useful and informative insights into the hyperthermia process.

Computer simulation of the hyperthermia process has been the topic of several studies since 1984 [15-18] until now [19-24]. The aim of these *in silico* studies is to find the temperature distribution throughout the cancer tumour tissue and its surrounding tissues. In some of these studies, a tissue phantom model with a regular geometric shape is also made and the temperature distribution in the tissue model is experimentally measured and its results are used to evaluate the computer simulation outputs [6, 25, 26].

In the present study, we have mathematically simulated the cell death rate resulted from the hyperthermia process as a function of temperature distribution in a spherical cancer tumor and its surrounding healthy tissue phantoms. The physical properties of brain cancer tumor and brain healthy tissues are used for the simulated phantoms. Solving the bio-heat equations, the temperature distribution across the cancer tumor and healthy tissue phantoms is obtained, and the amount of cell death for each tissue (correlated with the tissue phantom temperature) versus time and position within the tissues is calculated. The effects of heat dissipation amount from MNPs, the MNPs distribution pattern inside the tumor tissue phantom, and the hyperthermia process duration on the amount of cancerous and healthy cells death are investigated. To have a real value for the amount of heat released from MNPs, a simple experimental setup is designed and the amount of heat dissipation from synthesized magnetite (Fe_3O_4) nanoparticles is measured and used in the computer simulation. The results indicate that the generated heat is effective in destroying the cancerous cells with minimal destructive effect on the cells in the healthy tissue phantom.

2. Materials and methods
2.1. Magnetite (Fe_3O_4) MNPs preparation
The method developed by Chao Hui et al. [27] is adopted for synthesizing the magnetite nanoparticles. 36 g sodium nitrate ($NaNO_3$) and 0.3 g sodium hydroxide (NaOH) are dissolved into 40 ml distilled water at 90 ^{o}C. Then, 1.8 g Iron (II) oxide ($FeSO_4.4H_2O$) is added to the solution, and the solution is stirred at 90 ℃ for 20 minutes. By chilling the solution, the nanoparticles precipitate and the

solution color turns into dark brown. The precipitated nanoparticles are washed with distilled water, and then dispersed with ultrasonic probe for 30 minutes.

2.2. Heat dissipation measurement

To measure the heat dissipation amount from magnetite nanoparticles, a solution of Fe_3O_4 nanoparticles is prepared and put inside an alternating magnetic field generator (HF-H-ST 45, *Sadr Sanat Danesh* Metallurgical Industries Engineering Co. , Iran) shown in Fig. 1. The amount of heat dissipation per unit mass of the MNPs, called specific loss power (SLP), is measured by running the generator

at certain frequency and magnetic field strength and by measuring the solution temperature periodically. SLP correlates with periodic temperature measurements through the following equation [28]:

$$SLP = C_P . \frac{m_f}{m_m} . \frac{\Delta T}{\Delta t} \qquad (1)$$

where m_m and m_f are masses of magnetic nanoparticles and solution, respectively; C_P is the specific heat capacity of the solution, and $\Delta T / \Delta t$ is the slope of the temperature versus time curve which is measured at the very beginning of the experiment (i.e., at time zero).

Figure 1. Induction heating with an alternating magnetic field generator.

To simplify Eq. (1), some assumptions are taken into account. It is assumed that the solution heat capacity is equal to the water heat capacity (i.e., $C_P. = 4.185 \, J/g°C$) and the mass of solution is equal to the mass of pure water [28]. Since the water density is 1 g/ml, Eq. (2) can be rewritten as follows [29]:

$$SLP = C_P . \frac{1}{C_m} . \frac{\Delta T}{\Delta t} \qquad (2)$$

where C_m is the concentration of MNPs in solution.

2.3. Bio-heat mathematical model

The bio-heat equation is in fact the heat balance equations over the living tissues.

Several bio-heat equations are suggested in the literature and well reviewed in [30, 31], among which the Pennes equation is the widely used in several biological studies [32-35]. The Pennes equation is a partial differential equation expressing the heat balance over the living tissues as follows [36]:

$$\rho C \frac{dT}{dt} + \nabla . (-k\nabla T) = \rho_b C_b \omega_b (T_b - T) + Q_{met} + Q_{ext} \tag{3}$$

where ρ_b and ρ are the densities of the blood and tissue, respectively; k is the tissue thermal conductivity; C_b and C are the blood and tissue specific heat capacity, respectively; ω_b is the blood perfusion rate; T_b and T are the blood and tissue temperatures, respectively; Q_{met} is the heat sink/source by metabolic processes, and Q_{ext} is the heat generated in the tissue induced by external sources.

In the present study, since a phantom tissue model is used, the metabolic heat source and the heat transfer between the tissue and the blood vessels are assumed to be zero [37]. The physical properties of both tissues are indicated in Table 1.

Table 1.
Thermo-physical properties of tissues.

Materials	$k \left(\frac{W}{m\,K}\right)$	$\rho \left(\frac{kg}{m^3}\right)$	$C_p \left(\frac{J}{kg\,K}\right)$
Brain [38]	0.527	1050	3305
Brain tumor [39]	0.550	1047	3560

2.4. Cell survival model

Various models have been proposed and used for the rate of cell survival following heating [40-51] which are described and compared in [52]. These models correlate the amount of survived cells and the temperature of the living tissue following the hyperthermia process. The first-order model is a simple cell survival model with one parameter (α) which provides predictions of cell injury degree following a wide range of heating protocols [45]; due to its simplicity, generality, and sufficient accuracy, it has been widely used in various studies [45-51]. It expresses the fraction of survived cells in a living tissue as a function of the tissue injury degree due to thermal ablation through the following equation:

$$S = \exp(-\alpha) \tag{4}$$

where S is the fraction of survived cell with a value between 0 and 1, and α is the degree of tissue injury during the hyperthermia process. α correlates with the tissue temperature in the Arrhenius equation:

$$\frac{d\alpha}{dt} = A. exp(-\frac{E}{RT}) \tag{5}$$

where A is the frequency factor, and E is the activation energy for the irreversible damage reaction. These two parameters are dependent on the tissue type. For the present study, physical properties of the brain cancerous and healthy tissues are considered for the phantoms. The corresponding cell survival model parameters are shown in Table 2.

The fraction ratio of dead cells to the total

number of cells is also calculated by the following equation:

$$\theta_d = 1 - S = 1 - \exp(-\alpha) \qquad (6)$$

2.5. Tissue phantom model

The geometric shape of cancerous tumors is mostly spherical [55]; therefore, a sphere is usually considered to represent a tumor and a cylinder surrounding the sphere is considered to represent the healthy tissue for *in silico* studies [56-59]. This model is symmetric and the temperature changes only in the radial direction which simplifies the bio-heat equation solution. In some advanced

simulations, complex three-dimensional models representing the actual tumor obtained from MRI and CT images are considered [60-62].

The tissue phantom model considered here comprises two parts: a 10 mm radius sphere and a 30 mm radius cylinder with the height of 80 mm representing the tumor and its surrounding healthy tissue phantoms, respectively. A three-dimensional preview of the phantom model is shown in Fig. 2. For this phantom model, it is assumed that the temperature variations are independent of the angular position.

Table 2.

Parameters of the Arrhenius equation for both tissue phantoms.

Tissue type	$E\ (\dfrac{J}{mol})$	$A\ (s^{-1})$
Brain [53]	5.264×10^5	1.04×10^{84}
Brain tumor (clonogenic cells) [54]	5.064×10^5	2.984×10^{80}
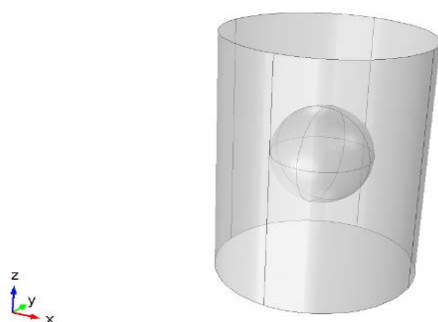
Figure 2. The two-part phantom model considered to represent the brain tumor and its surrounding healthy tissues.

3. Results
3.1. SLP of MNPs solution

To measure the SLP of the MNPs solution, a solution of 0.15 mg/ml of magnetite nanoparticles is prepared and exposed to an alternating magnetic field of 300 kHz with the field strength of 40 kA/m, and its temperature is measured every 1 minute. The experimental

results are shown in Fig. 3.

From Fig. 3 and Eq. (2), the SLP of the solution is calculated to be 140 W/g of MNPs.

3.2. The Pennes equation solution

Since a typical human body temperature in normal conditions is at 37 ^{o}C, the initial condition for the Pennes equation for both parts of the phantom model is:

$$T_{t=0} = 37\,°C \qquad (7)$$

For the boundary conditions, all outer surfaces of the cylinder are considered to be at the body temperature (i.e., 37 $°C$).

To evaluate the results of the computer simulation in detail, certain positions within the phantom model (five red points shown in Fig. 4) are determined arbitrarily where variations of the temperature and corresponding cells death rate versus time are obtained from the computer simulation. The radial positions of the points are 3, 6, 9, 11, 14 mm. The first three points are inside the tumor, and the last two points are in the surrounding healthy tissues.
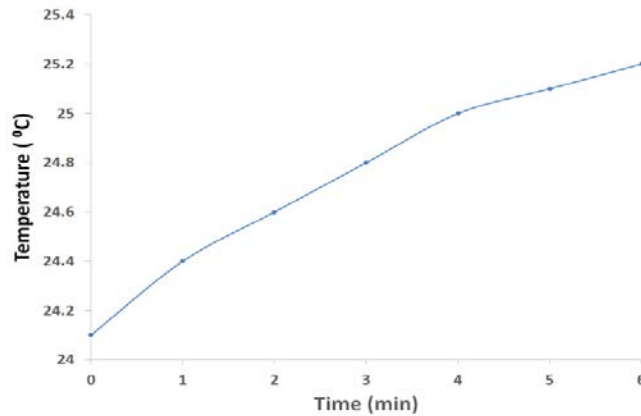
Figure 3. Nanofluid temperature variations versus time resulted from exposure to an alternating magnetic field of 300 kHz with the field strength of 40 kA/m.
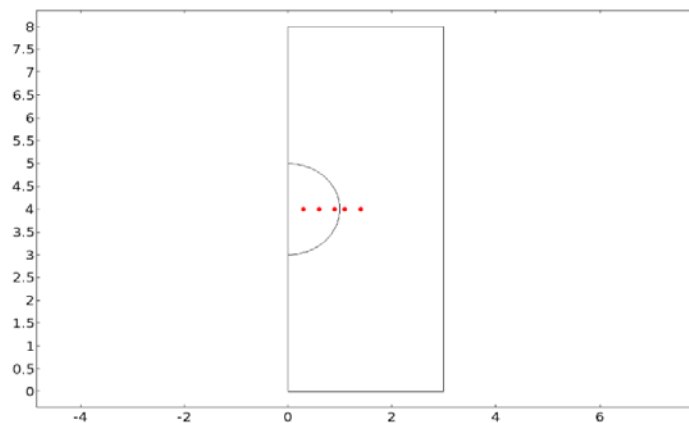
Figure 4. Certain positions where the variations of temperature and cells death rate versus time are obtained from the computer simulation.

To evaluate the effect of the heat dissipation amount from MNPs on the hyperthermia process, the process is simulated under three different amounts of heat dissipated from the MNPs. In general, the heat dissipation amount is a function of the MNPs chemical composition (Fe_3O_4 for the present study), the MNPs physical properties (i.e., concentration, mean diameter, and shape), and the magnetic field frequency and strength. Based on the calculated SLP for the synthesized magnetite nanoparticles, if, for instance, 2.85 mg of magnetite nanoparticles in a solution with the concentration of 0.15 mg/ml is exposed to an

alternating magnetic field of 300 kHz with the field strength of 40 kA/m, the amount of heat dissipated from the MNPs is 0.4 W. In Pennes equation, this value corresponds to Q_{ext}. Any change in every single one of the above factors would change the amount of heat dissipated from the magnetite nanoparticles. Regardless of what factor would change the heat dissipation amount, in the present study, three values of 0.3, 0.4, and 0.5 W for Q_{ext} are considered to simulate the hyperthermia process. These amounts can be due to any changes of the mentioned factors.

In addition to the simulation of various amounts of heat dissipation from MNPs, three possible scenarios for MNPs symmetric distribution patterns throughout the tumor are also simulated to indicate the impact of the MNPs distribution pattern on the hyperthermia process. In the first scenario, it is assumed that the MNPs are homogeneously distributed throughout the tumor. This scenario can be representative of multiple low-volume MNPs injections at different tumor sites, injection of MNPs at one site of the tumor's interstitial fluid space and distribution of MNPs throughout the whole tumor or injection of the MNPs into the arteries of a highly vascular tumor resulting in a homogenous distribution of MNPs throughout the tumor. In the second scenario, the MNPs are injected at the center of tumor and are distributed homogenously in an arbitrary sized sphere (here, 5 mm radius sphere is considered). This scenario represents injection of the MNPs at one site into the tumor's interstitial fluid space and the local distribution of MNPs within the tumor. In the last scenario, the MNPs are injected at the center of the tumor with no distribution throughout the tumor.

The variations of temperature and the fraction of dead cells in positions indicated in Fig. 4 for each scenario and for three different values of Q_{ext} are indicated in Figs. 5, 6, and 7.
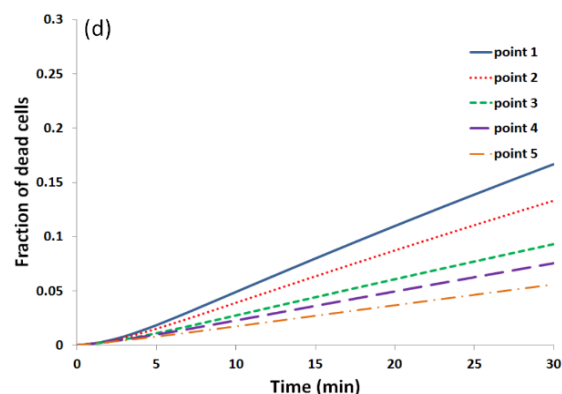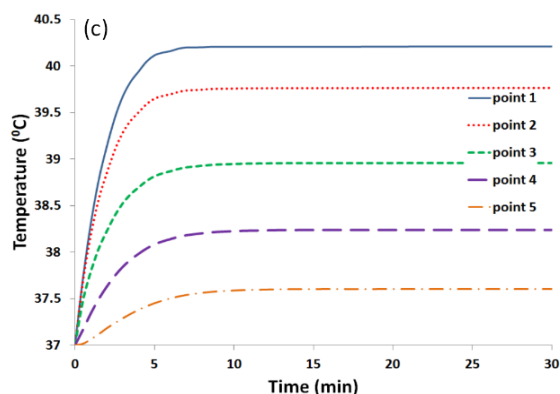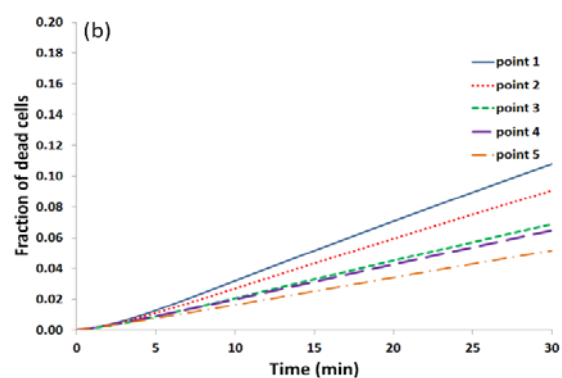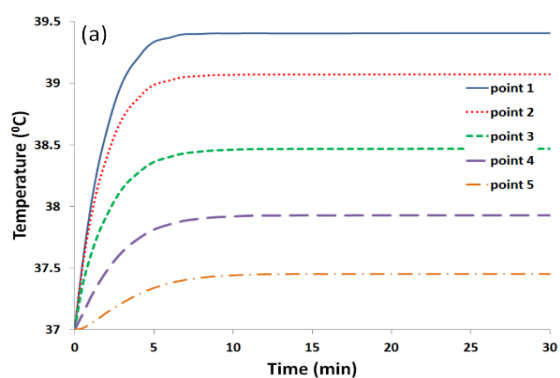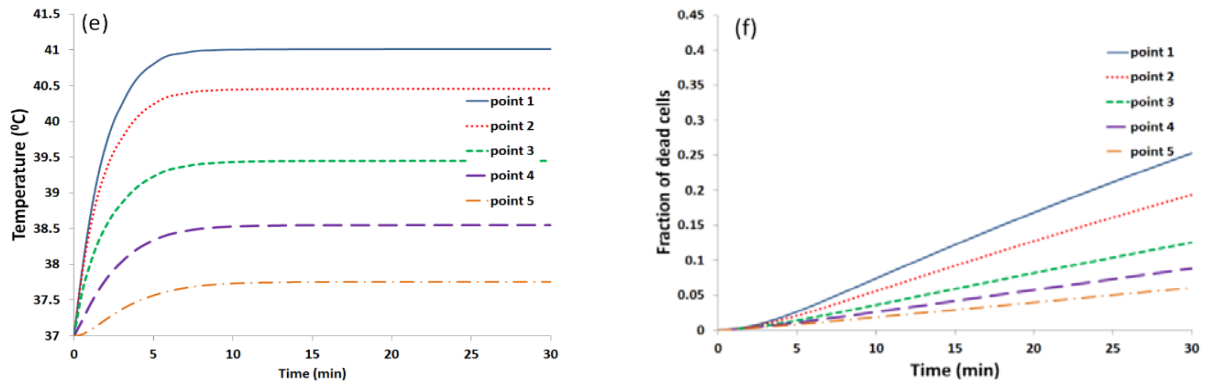
Figure 5. The variations of temperature and the fraction of dead cells versus time during the hyperthermia process of the first scenario at the positions shown in Fig. 4 for three different values of Q_{ext}, (a) and (b) $Q_{ext} = 0.3$ W, (c) and (d) $Q_{ext} = 0.4$ W, (e) and (f) $Q_{ext} = 0.5$ W.
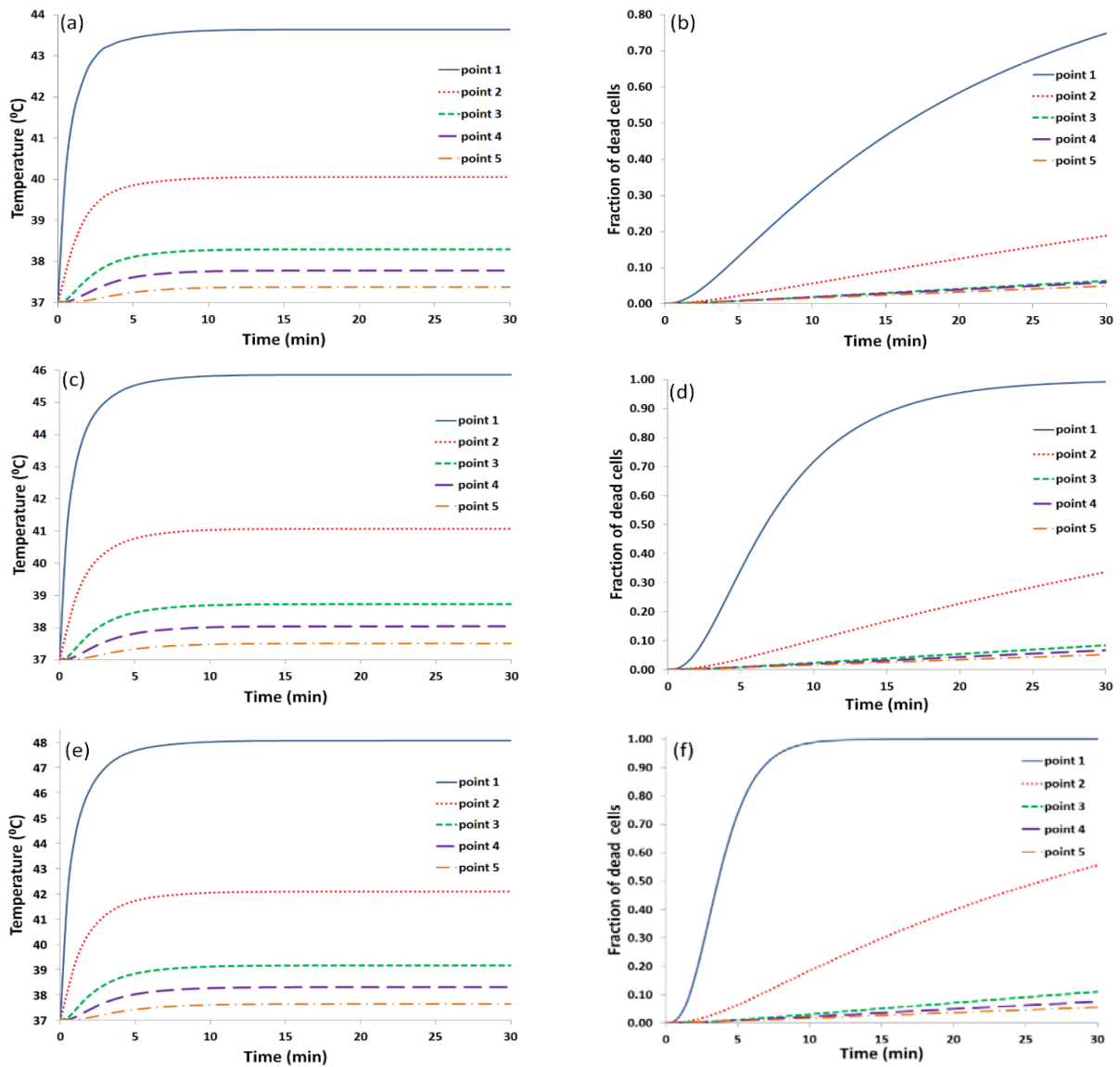
Figure 6. The variations of temperature and the fraction of dead cells versus time during the hyperthermia process of the second scenario at the positions shown in Fig. 4 for three different values of Q_{ext} (a) and (b) $Q_{ext} = 0.3$ W, (c) and (d) $Q_{ext} = 0.4$ W, (e) and (f) $Q_{ext} = 0.5$ W.
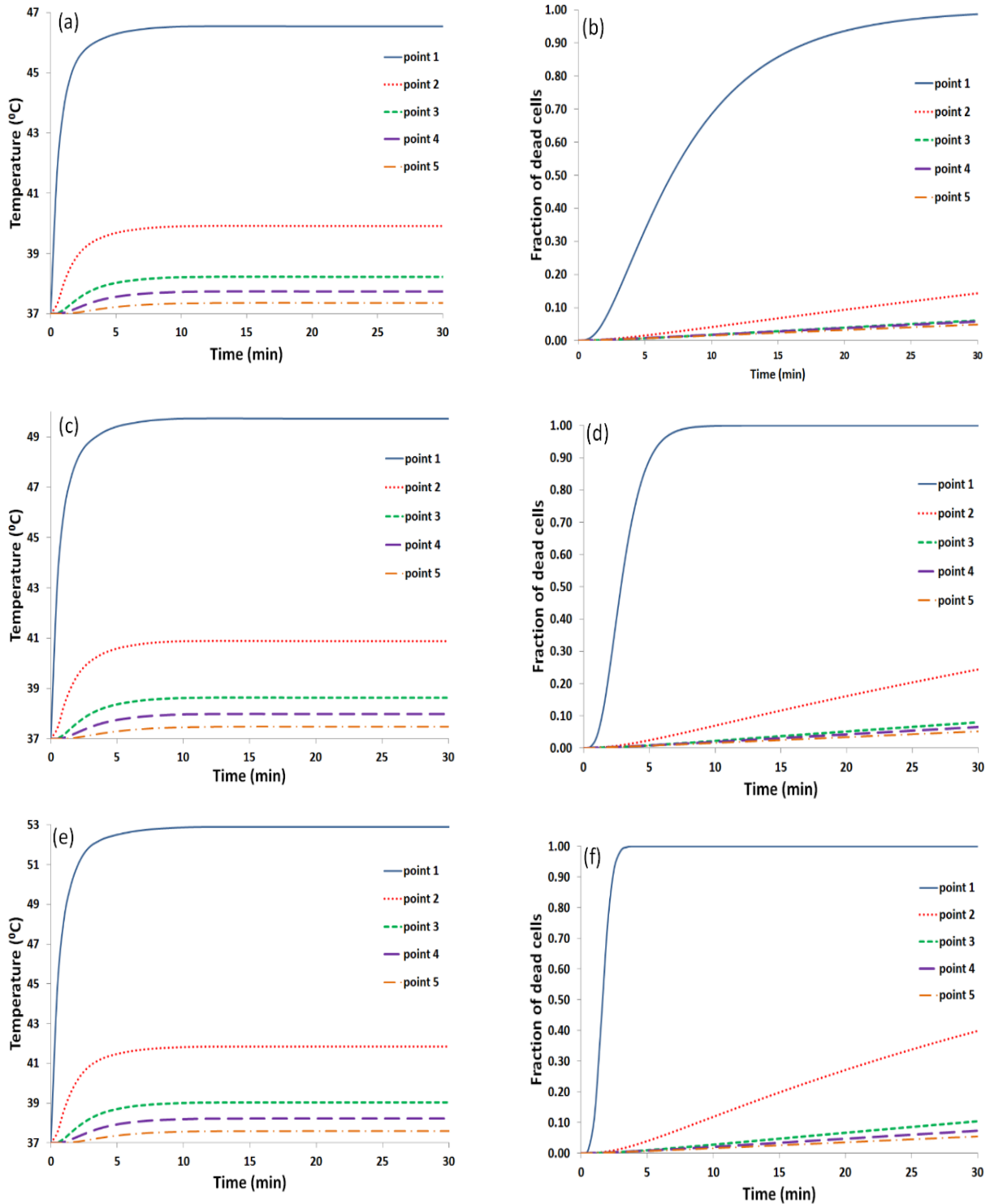
Figure 7. The variations of temperature and the fraction of dead cells versus time during the hyperthermia process of the third scenario at the positions shown in Fig. 4 for three different values of Q_{ext}, (a) and (b) $Q_{ext} = 0.3$ W, (c) and (d) $Q_{ext} = 0.4$ W, (e) and (f) $Q_{ext} = 0.5$ W.

The 2D temperature distributions and their corresponding fraction of dead cells for each scenario after 30 min of hyperthermia process for Q_{ext} of 0.5 W are shown in Fig. 8.

The average cell death rates of both cancerous and healthy tissues versus time for each scenario are also shown in Fig. 9.
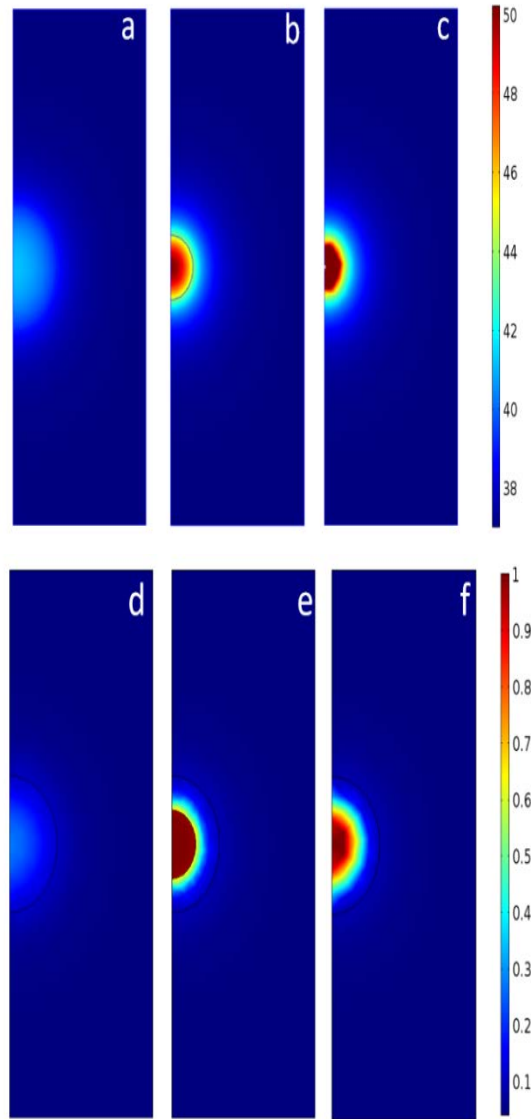
Figure 8. The 2-dimentional temperature distribution and its consequent dead cells fraction throughout the tumor and its surrounding healthy tissues after 30 min of hyperthermia process for Q_{ext}, of 0.5 W, (a) and (d) the first scenario, (b) and (e) second scenario, (c) and (f) third scenario.
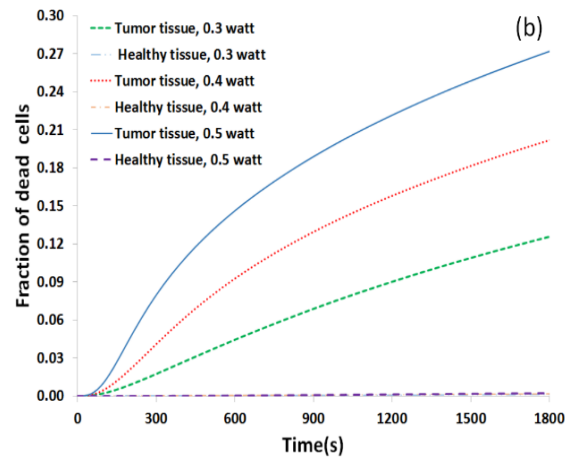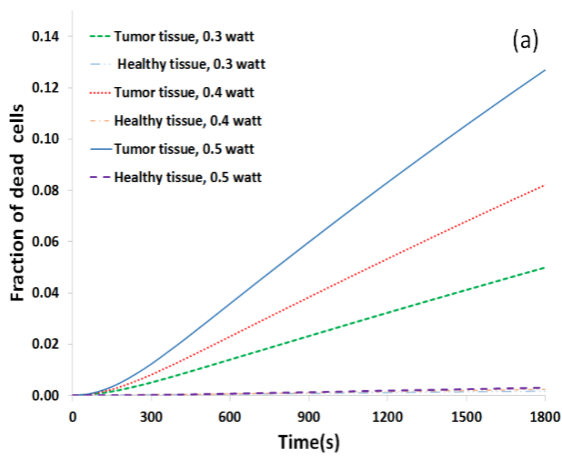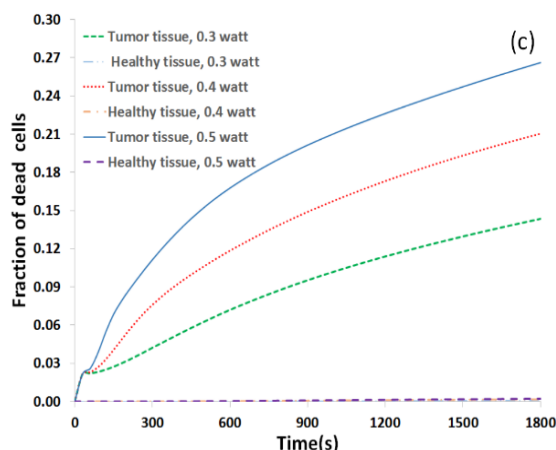
Figure 9. The average cell death rates of both cancer and healthy tissues versus time for the three considered MNPs distribution patterns under three different values of Q_{ext}, (a) first scenario, (b) second scenario and (c) third scenario.

4. Discussion

As implied by the results, in general, for all three scenarios of MNPs distribution patterns, the heat generated from the MNPs exposed to the alternating magnetic field increases the tissue temperature from 37 ^{o}C, and depending on the position within the tissue, the local tissue temperature reaches a new steady-state value after approximately 7 minutes. The closer to the center of the spherical tumor, the higher the steady-state temperature. The corresponding dead cell fraction also increases as a consequence of the elevated temperature, and depending on the position within the tissue, where the temperature is higher (which is maximum at the center of the spherical tumor), the corresponding local cell death rate is greater. Also, increasing the heat generation amount intuitively increases the cell death rate of the tumor and its surrounding healthy tissues for all distribution patterns.

4.1. First scenario

For this scenario, since the MNPs are homogenously dispersed throughout the whole tumor space, their concentration is diluted significantly; besides, the heat

generated from them is released in large volume. Therefore, the tumor temperature is not elevated remarkably. The temperature profile in the tumor and its surrounding tissues after 30 min of hyperthermia process (shown in Fig. 8) indicate that the maximum temperature at the center of the tumor is approximately 42 ^{o}C under Q_{ext} of 0.5 W. As Figs. 5 (a), (b) and (c) show, the local tumor temperature at point 1 reaches a maximum of 39.41 ^{o}C, 40.21 ^{o}C, and 41.01 ^{o}C corresponding to Q_{ext} of 0.3, 0.4 and 0.5 W, respectively, and the consequent dead cancerous cells fraction is not noticeable (similar results for points 2 and 3). Even by increasing the dissipated heat from MNPs, the cell death rate is still not satisfying. Moreover, the cell death rate in the surrounding healthy tissues is close to that of the tumor which is not tolerable since an acceptable thermotherapy should provide maximal cell death rate to the tumor tissue with minimal destruction to the surrounding healthy tissues.

4.2. Second scenario

Herein, more concentrated MNPs are present in the tumor since they are dispersed

homogenously in a smaller spherical space within the tumor (with respect to the previous scenario). Therefore, the generated heat is released in smaller volume within the tumor, diffuses through the surrounding portion of the tumor, and then diffuses through the surrounding healthy tissues. It is expected that the temperature at the central portion of the tumor be higher than that of the first scenario, and the tumor temperature at the outer portion (close to the boundary between the tumor and its surrounding healthy tissues) is less.

As expected, for the second scenario, the temperature at the center of the tumor reaches a steady-state value of approximately 49 ^{o}C under Q_{ext} of 0.5 W after being exposed to an alternating magnetic field for 30 minutes (see Fig. 8 (b)). The simulation results in Fig. 6 show that the local tumor temperature at point 1 reaches steady-state values of 43.64 ^{o}C, 45.85 ^{o}C, and 48.06 ^{o}C corresponding to Q_{ext} of 0.3, 0.4, and 0.5 W, respectively. On the other hand, the tissue temperature in the outer portion of the tumor (e.g., at point 3) reaches a steady-state value of 39.16 ^{o}C for Q_{ext} of 0.5 W. Comparing the steady-state temperature values at points 1, 3, 4, and 5 of the second scenario (i.e., 48.06 ^{o}C, 39.16 ^{o}C, 38.30 ^{o}C, and 37.64 ^{o}C for Q_{ext} of 0.5 W) to those of the first scenario (i.e., 41.01 ^{o}C, 39.45 ^{o}C, 38.55 ^{o}C, and 37.75 ^{o}C for Q_{ext} of 0.5 W) indicates that, under the identical condition of the hyperthermia process, the second scenario results in a very higher temperature at the central portion of the tumor with lower temperature at the outer portion of the tumor and its surrounding healthy tissues.

The consequent dead cells fraction in the tumor and its surrounding tissues indicate that the hyperthermia process is significantly destructive to the tumor cells residing within the tumor central portion. As Fig. 8 (e) shows,

for Q_{ext} of 0.5 W, almost all of the cancerous cells within the tumor central portion where MNPs are dispersed are killed, while partial cancerous cell death is achieved in other tumor portions. According to the simulation results indicated in Fig. 6 (f), the complete local cells death at point 1 occurs approximately after 12 min from the beginning of the hyperthermia process while partial cancerous cell death is achieved after 30 min of hyperthermia process in other points where MNPs are not present.

Figs. 9 (a) and (b) enable a quantitative comparison between the first and second scenarios. For Q_{ext} of 0.5 W, the first scenario results in an average of 12.69 % tumor cells death with 0.30 % of healthy cells death while the corresponding values for the second scenario are 27.20 % and 0.23 %, respectively. Therefore, the superiority of the second scenario is clear over the first one.

4.3. Third scenario
In this scenario, highly concentrated MNPs are considered to be present at the center of the tumor contained in a very small volume. When the tumor is exposed to the alternating magnetic field, it is expected to have a very high temperature at the center of the tumor due to the presence of highly concentrated MNPs. As Fig. 8 (c) shows, the temperature at the tumor center after 30 min of the hyperthermia process for Q_{ext} of 0.5 W is above 50 ^{o}C (temperatures above 50 ^{o}C are colored in white). Similar to what mentioned in the comparison of the second scenario with the first one, since the MNPs are only present in a tiny volume at the very center of tumor and are not dispersed into other parts of the tumor, it is expected to have higher temperatures at positions closer to the tumor center and lower temperatures at outer

portions of the tumor and at its surrounding healthy tissues with respect to the two previous scenarios. Comparing the steady-state temperature values at points 1 to 5 of the present scenario (i.e., 52.90 ^{o}C, 41.85 ^{o}C, 39.04 ^{o}C, 38.23 ^{o}C and 37.60 ^{o}C for Q_{ext} of 0.5 W) and their corresponding values of the second scenario (i.e., 48.06 ^{o}C, 42.09 ^{o}C, 39.16 ^{o}C, 38.30 ^{o}C and 37.64 ^{o}C for Q_{ext} of 0.5 W) satisfies this expectation. While this expectation was favorable in comparing the second and first scenarios, it may not be favorable in comparing the second and third scenarios. As mentioned earlier, an acceptable thermotherapy should impose maximum destructive effect on the tumor cells while keeping the healthy tissue cells undamaged. Therefore, comparing the resulted dead cells fractions of both scenarios would demonstrate the superiority of one to another.

Similar to the second scenario, herein, the hyperthermia process is also highly destructive to the cancerous tumor cells with low damage to the healthy tissue cells. What makes the third scenario different from the second one is the rate of tumor and healthy cells deaths. The rate of the cell destruction in the third scenario is faster in the central portion and is slower in the outer portion of the tumor with respect to those of the second scenario (see Figs. 6 and 7). In other words, the cells residing in the central portion of the tumor are completely killed in a few minutes after starting the hyperthermia process. For instance, considering the results in Figs. 6 (f) and 7 (f), after approximately 4 minutes of the hyperthermia process, all cells present within the 3 mm radius from the tumor center (i.e., the position of point 1) are completely killed, while the corresponding value for the second scenario is approximately 12 min. However, for the outer portion of the tumor (e.g., at

point 2), only 39.9 % of the cells at the radius of 6 mm are killed after 30 min of the hyperthermia process for Q_{ext} of 0.5 W, while this value is 55.6 % in case of the second scenario.

To make a better comparison, the results shown in Figs. 9 (b) and (c) are required to be assessed. For the third scenario, the very high rate of cell death at the tumor central portion dominates the low rate at the tumor outer portion at the beginning of the hyperthermia process. Moreover, the cell death rate at the tumor's very center is almost instantaneous. Therefore, the average cell death rates start with a sharp slope with non-zero value at the beginning of the hyperthermia process for all three values of Q_{ext}. Continuing the process, the slope of the curves reduces progressively. This trend differs from that of the second scenario. For that scenario, since the rate of the cells death in all tumor portions is neither very high nor very low, the curves have a moderate slope with a less progressive decrease. This difference makes the third scenario superior in destroying the tumor cells at the earlier times of hyperthermia process and less effective in later times. Comparing the results shown in Figs. 9 (b) and (c) when Q_{ext} is 0.5 W, for instance, for the first 23 min of hyperthermia process, the average tumor cell death resulted from the third scenario is superior to that of the second one, but after 23 min of the process, the cell destroying efficiency of the second scenario surpasses that of the third one. Regardless of the impact of time duration on the efficiency of the hyperthermia process, intuitively, more process duration results in more dead cells fraction of both tumor and healthy tissues for both scenarios. Depending on the tolerability of healthy tissue damage as well as the importance of resulted tumor dead cells

fraction, the efficient process duration varies. If small damages to the healthy tissues are tolerable, an objective function should be defined and the hyperthermia process duration can be prolonged until the objective function is optimized. If not, an amount threshold of healthy cell death determining the end point of the hyperthermia process must be considered.

5. Conclusions

In the present paper, we simulated a magnetic hyperthermia process in a cancer tumor and its surrounding healthy tissue mathematical phantoms. Bio-heat equations, besides the correlations, between the tissue temperature and the consequent cell death rate were solved. Considering the main objective of the hyperthermic therapy (i.e., a maximum damage to the cancer tumor with a minimal harm to the surrounding healthy tissues), the impact of the amount of dissipated heat from MNPs exposed to an alternative magnetic field, their distribution pattern inside the tumor and the hyperthermia process duration were investigated. It was indicated from the simulation results that the cell death rate is directly proportional to the amount of the released heat from the MNPs regardless of what factor would influence the heat amount. Nevertheless, what makes the hyperthermia process efficient is the MNPs distribution pattern. We examined three possible distribution patterns, and the simulation results indicated that homogeneous distribution of MNPs throughout the tumor is the least efficient distribution pattern since it leads to the low destruction of the tumor cells with a small damage to the surrounding healthy tissues. Two other distribution patterns (i.e., the local homogenous MNPs distribution and highly concentrated MNPs

with no distribution) resulted in significantly higher cell death rates in the cancer tumor with smaller damage to the surrounding healthy tissues with respect to that of the first distribution pattern. In comparison between the second and third MNPs distribution patterns, the simulation results indicated that highly concentrated MNPs at the very center of the tumor cause instantaneous cell death at the tumor center and very high cell death rate at the points close to the tumor center; however, it yields very low cell death rate at the outer tumor portion, while the second distribution pattern (i.e., local homogenous MNPs distribution) results in a not very high cell death rate at the tumor central portion and not very low cell death rate at the tumor outer portion. This difference made the third scenario with respect to the second scenario superior at the earlier times of the hyperthermia process, since it led to a higher average cell death rate in the whole tumor and inferior at the later times of the process.

References

[1] Xiaoming Li, J. W., Aifantis, K. E., Fan, Y., Feng, Q., Cui, F. Z. and Watari, F., "Review article: Current investigations into magnetic nanoparticles for biomedical applications", *Journal of Biomedical Materials Research, Part A,* **104** (5), 1285 (2016).

[2] Mahdi Karimi, A. G., Sahandi Zangabad, P., Rahighi, R., Moosavi Basri, S. M., Mirshekari, H., Amiri, M., Shafaei Pishabad, Z., Aslani, A., Bozorgomid, M., Ghosh, D., Beyzavi, A., Vaseghi, A., Aref, A. R., Haghani, L., Bahramian, S. and Hamblin, M. R., "Review article: Smart micro/nanoparticles in stimulus-responsive drug/gene delivery systems", *Chemical Society Reviews,* **45** (5), 1457

(2016).

[3] Hudson, R., "Reveiw article: Coupling the magnetic and heat dissipative properties of Fe_3O_4 particles to enable applications in catalysis, drug delivery, tissue destruction and remote biological interfacing", *RSC Advances,* **6** (5), 4262 (2016).

[4] Franziska Henrich, H. R. and Odenbach, S., "Heat transition during magnetic heating treatment: Study with tissue models and simulation", *Journal of Magnetism and Magnetic Materials,* **380**, 353 (2015).

[5] Ihab M. Obaidat, B. I. a. Y. H., "Review magnetic properties of magnetic nanoparticles for efficient hyperthermia", *Nanomaterials,* **5** (63-89), (2015).

[6] Manuel Bañobre-Lópeza, A. T. and Rivasa, J., "Review magnetic nanoparticle-based hyperthermia for cancer treatment", *Reports of Practical Oncology & Radiotherapy,* **18** (6), 397 (2013).

[7] W. Andra, H. N., Magnetism in medicine: A handbook, 1st ed., Wiley-VCH, (1998).

[8] Renato Cavaliere, E. C. C. and Giovanella, B. C., "Selective heat sensitivity of cancer", (May 15, 1967).

[9] K. Motomura, M. I., Komoike, Y., Koyama, H., Inaji, H., Inoue, M., Nagae, H. and Nagano, I., "Novel thermal tumor ablation for breast cancer in mice using magnetic nanoparticles", *Cancer Research*, 1916 (2009).

[10] Rhythm R. Shah, T. P. D., Glover, A. L., Nikles, D. E. and Brazel, C. S., "Impact of magnetic field parameters and iron oxide nanoparticle properties on heat generation for use in magnetic hyperthermia", *Journal of Magnetism and Magnetic Materials,* **387**, 96 (2015).

[11] P. Wust, J. N., Felix, R., Deuhard, P., John, W. and Louis., A., "Numerical approaches to treatment planning in deep RF-hyperthermia", *International Journal of Hyperthermia,* **7**, 157 (1991).

[12] P. Wust, J. N., Felix, R., Deuhard, P., John, W. and Louis., A., "Numerical approaches to treatment planning in deep RF-hyperthermia", *Strahlenther. Onkol,* **165**, 751 (1989).

[13] Cetas, R. B. R. a. T. C., "Applications of bioheat transfer simulations in hyperthermia", *Cancer Research,* **44**, 4788 (1984).

[14] Dinesh Kumar, K. N. R., "A study on thermal damage during hyperthermia treatment based on DPL model for multilayer tissues using finite element Legendre wavelet Galerkin approach", *Journal of Thermal Biology*, (2016).

[15] Alexander LeBrun, R. M. and Zhu, L., "MicroCT image based simulation to design heating protocols in magnetic nanoparticle hyperthermia for cancer treatment", *Journal of Thermal Biology*, (2016).

[16] Sazgarnia, A. N. N., Mehdizadeh, H. and Shahamat, Z., "Investigation of thermal distribution for pulsed laser radiationin cancer treatment with nanoparticle-mediated hyperthermia", *Journal of Thermal Biology,* **47**, 32 (2015).

[17] Ayani, M. B., "Source term prediction in a multilayer tissue during hyperthermia", *Journal of Thermal Biology,* **52**, 187 (2015).

[18] Cuschieri, Z. W. I. A. M. G. D. L. H. L. L. M. L. D. M. S. C. S. B. A., "Image-based 3D modeling and validation of radiofrequency interstitial tumor ablation using a tissue-mimicking breast

phantom", *International Journal of Computer Assisted Radiology and Surgery,* **7**, 941 (2012).

[19] Makoto Suto, H. K., Maruta, K., Ohta, M., Tohji, K. and Jeyadevan, B., "Heat diffusion characteristics of magnetite nanoparticles dispersed hydro-gel in alternating magnetic field", *Journal of Magnetism and Magnetic Materials,* **321**, 3483 (2009).

[20] Chao Hui, C. S., Yang, T., Bao, L., Tian, J., Ding, H., Li, C. and Gao, H.-J., "Large-scale Fe_3O_4 nanoparticles soluble in water synthesized by a Facile method", *Journal of American Chemical Society,* **112**, 11336 (2008).

[21] Antonios Makridis, K. T., Tziomaki, M., Sakellari, D., Simeonidis, K., Angelakeris, M., Yavropoulou, M. P., Yovos, J. G. and Kalogirou, O., "In vitro application of Mn-ferrite nanoparticlesas novel magnetic hyperthermia agents", *Journal of Materials Chemistry B,* (2013).

[22] Ritchie Chen, M. G. C. a. P. A., "Maximizing hysteretic losses in magnetic ferrite nanoparticles via model-driven synthesis and materials optimization", *ACS Nano (ACS Publications),* **7** (10), 8990 (2013).

[23] H. P. Kok, J. G., van den Berg, C. A. T., Stauffer, P. R., Hand, J. W. and Crezeel, J., "Thermal modelling using discrete vasculature for thermal therapy: A review", *International Journal of Hyperthermia,* **29** (4), 336 (2014).

[24] Tzu-Ching Shih, H.-S. K., Liauh, C.-T. and Lin, W.-L., "Thermal models of bioheat transfer equations in living tissue and thermal dose equivalence due to hyperthermia", **14** (2), (2002).

[25] Miller, M. M. S. a. D. F., "Nonlinear model for magnetic nanoparticle-based hyperthermia", *Int. J. Mathematical Modelling and Numerical Optimisation,* **6** (3), 223 (2015).

[26] Antonio Cervadoro, C. G., Pande, R., Sarangi, S., Preziosi, L., Wosik, J., Brazdeikis, A., Decuzzi, P., "Design maps for the hyperthermic treatment of tumors with superparamagnetic nanoparticles", *Plos One (open access),* (2013).

[27] M. Lahonian, A. A. G., "Research article: The effect of magnetic nanoparticle dispersion on temperature distribution in a spherical tissue in magnetic fluid hyperthermia using the lattice Boltzmann method", *International Journal of Hyperthermia,* **27** (3), 266 (2011).

[28] Pennes, H. H., "Analysis os tissue and artterial blood temperatures in the resting human forearm", *Applied Physiology,* **1**, (August 1948).

[29] Man Zhang, Z. Z., Wu, S., Lin, L., Gao, H. and Feng, Y., "Simulation of temperature field for temperature-controlled radio frequency ablation using a hyperbolic bioheat equation and temperature-varied voltage calibration: A liver-mimicking phantom study", *Journal of Physics in Medicine & Biology,* **60**, (2015).

[30] Holmes, P. K. R., "Thermal conductivity data for specific tissues and organs for humans and other mammalian species", T*he University of Texas at Austin*, (2009).

[31] Verga, D. S. a. N., "Cancer treatment with hyperthermia", *Novel Beyond Conventional Approaches*, (2011).

[32] Wright, N. T., "Parameter correlation in models of hyperthermic cell death",

ASME 2011 Summer Bioengineering Conference, 117 (2011).

[33] Yusheng Feng, J. T. O. a. M. N. R., "A two-state cell damage model under hyperthermic conditions: Theory and in vitro experiments", *Journal of Biomechanical Engineering,* **130** (4), (2008).

[34] Dewey, W. W. C., "Variation in sensitivity to heat shock during the cell-cycle of chinese hamster cells in vitro", *International Journal of Radiation Biology and Related Studies in Physics, Chemistry and Medicine,* **19** (5), 467 (1971).

[35] Rylander, M. N., Feng, Y., Zimmermann, K. and Diller, K. R., "Measurement and mathematical modeling of thermally induced injury and heat shock protein expression kinetics in normal and cancerous prostate cells", *Int. J. Hyperthermia,* **26** (8), 748 (2010).

[36] Feng, Y., Tinsley Oden, J. and Rylander, M. N., "A two-state cell damage model under hyperthermic conditions: Theory and in vitro experiments", *J. Biomech. Eng.,* **130** (4), 410 (2008).

[37] Henle, K. J. and Dethlefsen, L. A., "Time-temperature relationships for heat-induced killing of mammalian cells", *Ann. N. Y. Acad. Sci.,* **335**, 234 (1980).

[38] Ratovoson, D., Huon, V. and Jourdan, F., "A 3D finite element model for hyperthermia injury of blood-perfused skin", *Comput. Methods Biomech. Biomed. Engin.,* **18** (3), 233 (2015).

[39] Wright, N. T., "Comparison of models of post-hyperthermia cell survival", *Biomechanical Engineering,* **135**, 510 (2013).

[40] Weiswald, L. B., Bellet, D. and Dangles-Marie, V., "Spherical cancer models in tumor biology", *Neoplasia,* **17** (1), 1 (2015).

[41] Henrich, F., Rahn, H. and Odenbach, S., "Heat transition during magnetic heating treatment: Study with tissue models and simulation", *Journal of Magnetism and Magnetic Materials,* **380**, 353 (2015).

[42] Attar, M. M., Haghpanahi, M., Amanpour, S. and Mohaqeq, M., "Analysis of bioheat transfer equation for hyperthermia cancer treatment", *Journal of Mechanical Science and Technology,* **28** (2), 763 (2014).

[43] Suto, M., Kosukegawa, H., Maruta, K., Ohta, M., Tohji, K. and Jeyadevan, B., "Heat diffusion characteristics of magnetite nanoparticles dispersed hydro-gel in alternating magnetic field", *Journal of Magnetism and Magnetic Materials,* **321** (20), 3483 (2009).

[44] Wang, Z., Aarya, I., Gueorguieva, M., Liu, D., Luo, H., Manfredi, L., Wang, L., McLean, D., Coleman, S., Brown, S. and Cuschieri, A., "Image-based 3D modeling and validation of radiofrequency interstitial tumor ablation using a tissue-mimicking breast phantom", *Int. J. Comput. Assist. Radiol. Surg.,* **7** (6), 941 (2012).

[45] LeBrun, A., Ma, R. and Zhu, L., "MicroCT image based simulation to design heating protocols in magnetic nanoparticle hyperthermia for cancer treatment", *Journal of Thermal Biology,* **62**, Part B, 129 (2016).

[46] Lebrun, A., Manuchehrabadi, N., Attaluri, A., Wang, F., Ma, R. and Zhu, L., "MicroCT image-generated tumour geometry and SAR distribution for tumour temperature elevation simulations in magnetic nanoparticle

hyperthermia", *Int. J. Hyperthermia,* **29** (8), 730 (2013).

[47] Bin Xie, R. S., Torti, F. M., Keblinski, P. and Torti, S., "Heat localization for targeted tumor treatment with nanoscale near-infrared radiation absorbers", *Physics in Medicine and Biology,* **57** (18), 5765 (2013).

[48] Pearce, J. A., "Improving accuracy in Arrhenius models of cell death: Adding a temperature-dependent time delay", *Journal of Biomechanical Engineering,* **137**, (2015).